Numerical experiments of Full Waveform Inversion on a typical Pre-Salt Model. Part 3: 3D effects

Bruno Pereira-Dias, André Bulcão, Djalma Manoel Soares Filho, Eldues Oliveira Martins, Felipe Prado Loureiro, Felipe de Souza Duarte, Luiz Alberto Santos, PETROBRAS

Abstract

In this paper, we apply our Full Waveform Inversion and Reverse Time Migration scheme to investigate 3D effects on 2D algorithms. Since the used algorithms for inversion and migration are 2D, it is realized a study for phase and amplitude correction from 3D to 2D data. This can be a guide for utilizing FWI in complex models. We observe that a robust objective function and 3D amplitude correction that takes into account velocity variation in the media, yields the best inversion results. For the numerical examples we use a representative pre-salt model based on Santos Basin, offshore Brazil. Both 2D and 3D data the velocity models obtained from FWI results in better focus and definition of the migrated image, especially in the pre-salt region.

Introduction

Full waveform inversion is among the most important tools for seismic exploration and hydrocarbon reservoir characterization. It has the potential of improving the resolution dramatically in comparison to traditional seismic imaging techniques. Its secret is the use of propagating events as a whole, along with primaries, surface related and internal multiples, converted waves etc. However, much has to be done in order to have FWI as tool shelf due to high computational cost and the presence of local minima induced by cross-talks that arise from non-related events.

This class of technologies for inversion that involve the full wavefield demand adequate amplitude and phase of the modeling scheme. In this vein, we compare the propagation of acoustic waves in 2D and 3D in a representative Santos Basin pre-salt synthetic model.

This work is a continuation of (Souza et al., 2013) and (Pereira-Dias et al. 2014), where the primer analysed the stability of the FWI in relation to initial velocity field of a typical pre-salt model was analysed by numerical experiments and the former investigated elastic effects in an acoustic FWI algorithm.

Converting 3D data to 2D

It is widely known that there is a great difference between 2D and 3D propagation of the seismic wavefield due to geometrical spreading and the Green's function solution (see for example (Ikelle and Amundsen, 2005)). Figure 1 show this amplitude and phase difference for a homogeneous medium

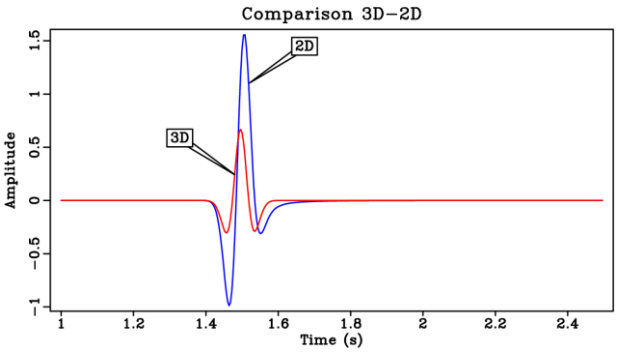

Figure 1 Comparison of the seismic record for 3D and 2D propagation in a homogenous medium (v=1500m/s).

To mitigate these differences, one can consider the Green's functions for 3D and 2D in frequency domain for a homogeneous media

$$G_{3D}(\mathbf{r},\omega)=\frac{1}{4\pi r}\exp\left[i(\omega r/c)\right], \quad (1)$$

$$G_{2D}(\mathbf{r},\omega)=\sqrt{\frac{1}{8\pi}}\sqrt{\frac{1}{r/c}}\frac{1}{\sqrt{-i\omega}}\exp\left[i(\omega r/c)\right] \quad (2)$$

The relationship between (1) and (2) is

$$G_{2D}(\mathbf{r},\omega)=G_{3D}(\mathbf{r},\omega)\sqrt{\frac{2\pi\sigma}{-i\omega}}, \quad (3)$$

where σ is defined as $\sigma=cr$ for a constant velocity medium.

The product in equation (3) corresponds to the causal half-integration $D_{-1/2}$ (Deregowski and Brown, 1983) operator by a factor of $\sqrt{2\pi\sigma}$. In time domain, this operation takes the form of a convolution with $D_{-1/2}=F\left\{(-i\omega)^{-1/2}\right\}=H(t)/\sqrt{t}$, where $H(t)$ is the Heaviside function. This yield to

$$G_{2D}(\mathbf{r},t) = \sqrt{2\pi\sigma}\, D_{-1/2}\{G_{3D}(\mathbf{r},t)\} = \sqrt{2\pi\sigma}\left[\frac{H(t)}{\sqrt{t}} * G_{3D}(\mathbf{r},t)\right]. \quad (4)$$

For a medium with varying velocity, σ is the integration of velocity *w.r.t.* arc length *s* of the ray trajectory (Bleinstein et al, 2001).

$$\sigma = \int_s c(s)ds \quad (5)$$

For a piecewise homogeneous medium and 1D approximation, the expression can be simplified to

$$\sigma = \sum_{i=1}^{n} v_i s_i = \sum_{i=1}^{n} v_i^2 \Delta t_i = v_{rms}^2(t); \quad (6)$$

$$v_{rms}(t) = \sqrt{\frac{\sum_{i=1}^{n} v_i^2 \Delta t_i}{\sum_{i=1}^{n} \Delta t_i}}\ ;\ t = \sum_{i=1}^{n} \Delta t_i \quad (7)$$

Thus, converting data down from 3D to 2D, limited to media with smoothly varying velocity and small angles may be stated as

$$G_{2D}(\mathbf{r},t) = \sqrt{2\pi t}\, v_{rms}(t) D_{-1/2}\{G_{3D}(\mathbf{r},t)\} \quad (8)$$

This correction is applied to the FWI problem in references (Wang and Rao, 2009; Prebindowska, 2013).

In order to measure up amplitude and phase correctness between 3D and 2D data, we consider the 3D modeling using the 2.5D Jupiter model (Figures 2 and 3). The 2.5D model is used to avoid the influence a more geologically complex 3D model would have due to sideways spreading.
For this comparison, we use as reference the seismogram come from shot number 50 (Fig. 5). Three distinct corrections were applied:

- Correction 1: $\sqrt{t} D_{-1/2}(t)$
- Correction 2: $v_{rms,zo}(t)\sqrt{t} D_{-1/2}(t)$
- Correction 3: $v_{rms,cmp}(t)\sqrt{t} D_{-1/2}(t)$.

The second type takes the rms velocity of the zero offset trace into account, while the third takes the rms velocity at the trace common midpoint instead. The first type, although it takes a velocity to be constant, is widely referenced to in literature (Crase et al. 1990; Zhou et al. 1995; Hicks and Pratt, 2001; Shipp and Singh, 2002; Operto et al, 2006). Type 2 is used in (Wang and Rao, 2009; Prebindowska, 2013).

Figure 7 shows the residue between reference seismogram and the three types of correction. As expected, types 2 and 3 were better able at correcting both near and far offsets. Yet they fail around overlaping events, which is evident where post-critical events cross the direct wave.

Full Waveform Inversion

FWI departs from the definition of an objective function, comparing modeled to observed data. One might consider, for instance, the objective function to be the L2-norm of such discrepancy.

$$E_{L2}(m) = \frac{1}{2}\sum_{s=1}^{N_S} \|u_s(m) - d_s\|^2 . \quad (9)$$

Objective function defined, a local optimization scheme should update the model. Using the gradient method, model update is given by

$$m_k = m_{k-1} - \alpha \nabla E(m), \quad (10)$$

Where the gradient can be approximated by the adjoint method (Fitchner, 2011)

$$\nabla E(m) = \sum_{s=1}^{N_S} \int_0^T \frac{\partial^2}{\partial t^2} u_s(t) v_s(t) dt , \quad (11)$$

with $u(t)$ being the forward modeled propagation field and $v(t)$ the adjoint modeled field, one which is spread backwards in time and which source $u_s(m) - d_s$ is defined at acquisition geometry. The value α is set by a linear search technique.

A criterion of weighted L2-norm is proposed by (Choi and Alkhalifah 2013) as

$$E_{L2-rms} = \frac{1}{2}\sum_{s=1}^{N_S}\left[\frac{u_s(\mathbf{m})}{\|u_s(\mathbf{m})\|} - \frac{d_s}{\|d_s\|}\right]^2 , \quad (12)$$

where both denominators are the RMS value of each trace, respectively from modeled and observed data. The first denominator is defined as

$$\|u_s^j(\mathbf{m})\| = \sqrt{\frac{1}{NT}\sum_{k=1}^{NT} u^k(\mathbf{m})^2}\ , j = 1,...,ntr . \quad (13)$$

It is expected that this objective function is more robust to amplitude errors since it can compensate errors not contemplated by 3D to 2D correction.

Examples

The numerical examples are realized on a synthetic model shown in Figure 2. The modeled dataset was realized by 3D and 2D finite difference acoustic modeling engines.

Figure 3 shows the 2.5D model, with consist in the repetition of a 2D model along the y direction. The exact model is show on Figure 4 and the initial model for inversion is given in Figure 5.

The FWI algorithm was realized on the time domain. It was also used multi-scale technique by frequency bandwidth and source-receiver offset, so to avoid

convergence to a local minimum. The inversion parameters are described in Table 1.

Table 1: Inversion parameters

Grid point interval	25 m
Initial inversion frequency	6Hz
Final inversion frequency	12 Hz
Inversion frequency interval	2 Hz
Initial inversion offset	4000m
Final inversion offset	16000m
Inversion offset interval	4000m

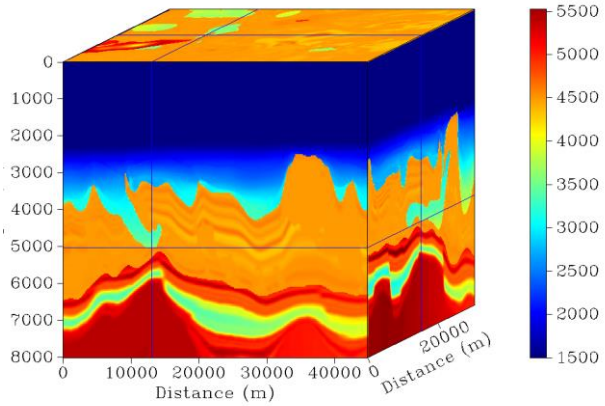

Figure 2: 3D Velocity Model. The y-direction slice show the complex salt geometry for this model.

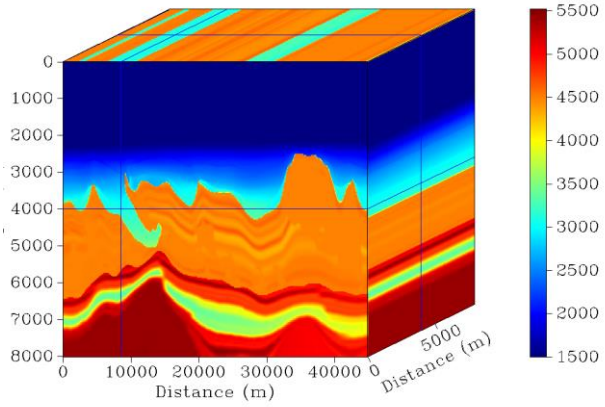

Figure 3: 2.5D Velocity Model used for amplitude calibration and testing.

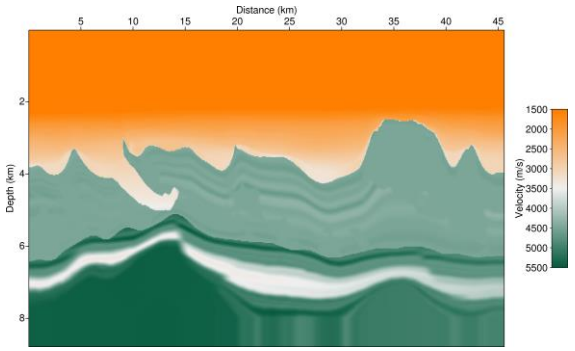

Figure 4: 2D slice of exact model.

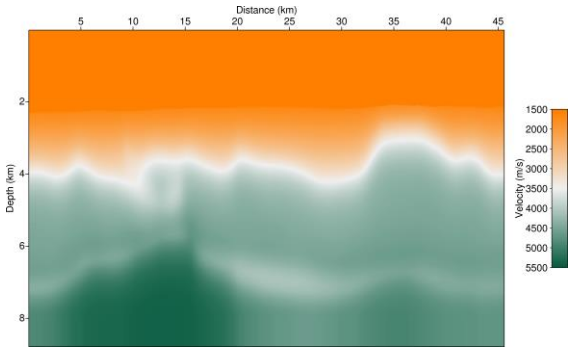

Figure 5: Initial model for inversion. It is a smoothed version of exact model by smoothing the slowness with a radius of 1000m.

Results

Figure 6 shows the result from a fully 2D process (data, modeling, inversion) which we consider as benchmark. Figure 8 shows what the results are like when disregarding a proper velocity correction and using a less robust minimization criterion. Further figures demonstrate the benefits of both velocity correction and minimization scheme (Figure 9).

A comparison of the different amplitude correction and objective function are present in Figure 9. One can conclude that the use of a more robust objective function that deals with normalized residuals yields the best results for 2.5D and 3D.

Another criteria to show the benefits of the inversion obtained is by the migration results. The models used for migration were the initial model (Figure 5) and the obtained result for inversion (Figure 6, Figure 9e and Figure 9f). All the cases, 2D, 2.5D and 3D, there is benefit of the use of FWI model.

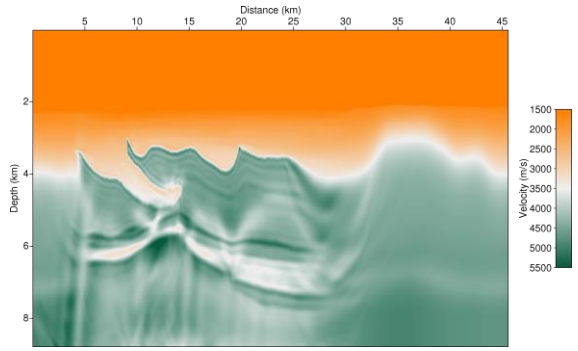

Figure 6: 2D FWI result for 2D data. This is the reference FWI to be used for comparisons.

Conclusions

This paper proposed corrections for amplitude and phase in the propagation of acoustic wave in 2D and 3D media. These corrections were used in 3D synthetic data for 2D inversion algorithms. The results show that utilizing a robust objective function (RMS normalized L_2-norm) and 3D amplitude correction that takes into account the medium velocity yields better results.

However, the need of using 3D migration and inversions algorithms remains clear. In fact, lateral scattering and inaccuracies in the 3D correction for crossing events in the shot-gathers are not contemplated in 2D approaches. Albeit the greater computational cost, 3D modeling and inversion algorithms ought to give better inversion results, especially for models which presents the characteristics of Santos Basin.

Acknowledgments

The authors would like to thank PETROBRAS for authorizing this publication.

References

N. Bleinstein, J. K. Cohen, and J. W. Stockwell Jr. Mathematics of Multidimensional Seismic Imaging,
Migration, and Inversion. Springer, 2001.

Y. Choi and T. Alkhalifah. Multisource waveform inversion of marine streamer data using normalized wavefield.
Geophysics, **78**(5):R.197_R206, September-October 2013.

E. Crase, A. Picat, M. Noble, J. McDonald, and A. Tarantola. Robust elastic nonlinear waveform inversion:
Application to real data. Geophysics, **55**(2):527_538, 1990.

S. M. Deregowski and S. M. Brown. A theory of acoustic difractors applied do 2-d models. Geophysical Prospecting, **31**:293-333, 1983.

A. Fichtner. Full Seismic Waveform Modelling and Inversion. Springer, 2011.

G. J. Hicks and R. G. Pratt. Reflection waveform inversion using local descent methods: Estimating attenuation and velocity over a gas-sand deposit. Geophysics, **66**(2):598_612, March-April 2001.

L. T. Ikelle and L. Amundsen. Introduction to Petroleum Seismology (Investigations in Geophysics no. 12).
Society of Exploration Geophysicists, 2005.

J. Miksat, T. M. Müller, and F. Wenzel. Simulating three-dimensional seismograms in 2.5-dimensional structures
by combining two-dimensional finite difference modelling and ray tracing.Geophysical Journal International,
174:309-315, 2008.

P. M. Morse and H. Feshbach. Methods of Theoretical Physics. McGraw-Hill Science/Engineering/Math., 1953.

S. Operto, J. Virieux, J.-X. Dessa, and G. Pascal. Crustal seismic imaging from multifold ocean bottom
seismometer data by frequency domain full waveform tomography: Application to the eastern nankai trough. Journal of Geophysical Research, **111**:B09306, 2006.

B. Pereira Dias, A. A. V. B. Souza, A. Bulcão, D. M. Soares Filho, F. F. Farias, F. P. Loureiro, L. A. Santos,
Numerical experiments of full waveform inversion on a typical pre-salt model. Part 2: Elastic Effects, 76th EAGE Conference & Exhibition 2014

A. Przebindowska. Acoustic Full Waveform Inversion of Marine Re_ection Seismic Data. PhD thesis, Karlsruher Instituts für Technologie, 2013.

R. M. Shipp and S. C. Singh. Two-dimensional full wavefield inversion of wide-aperture marine seismic streamer data. Geophysical Journal International, **151**:325_344, 2002.

A. A. V. B. Souza, A. Bulcão, B. Pereira-Dias, D. M. Soares Filho, E. Martins, F. F. Farias, F. P. Loureiro, G. C. Alves, L. A. Santos, R. F. C. C. da Cruz. Numerical experiments of Full Waveform Inversion on
a typical Pre-Salt Model. Part 1: stability in relation to initial velocity field Thirteenth International Congress of the Brazilian Geophysical Society, 2013

Y. Wang and Y. Rao. Reflection seismic waveform tomography. Journal of Geophysical Research, **14**:B03304, 2009.

C. Zhou, W. Cai, V. Luo, G. T. Schuster, and S. Hassanzadeh. Acoustic wave-equation inversion of crosshole seismic data. Geophysics, **60**(3):765-773, 1995.

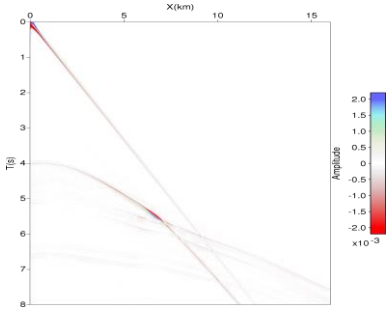

(a) Residue correction 1

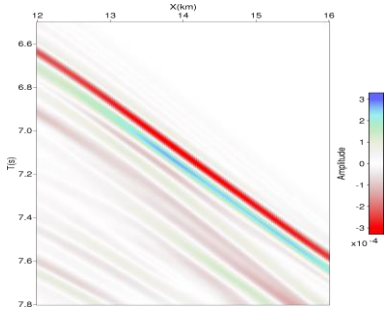

(b) Residue correction 1 (far)

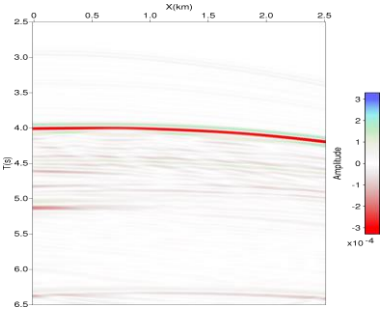

(c) Residue correction 1 (near)

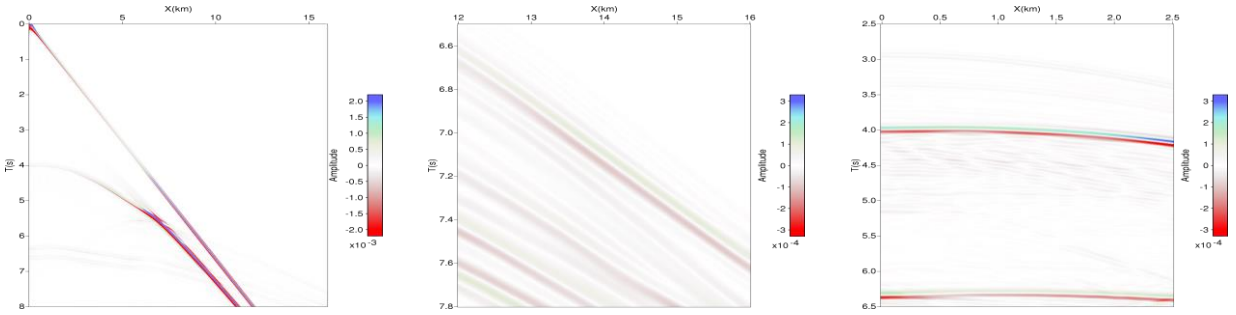

(d) Residue correction 2 (e) Residue correction 2 (far) (f) Residue correction 2 (near)

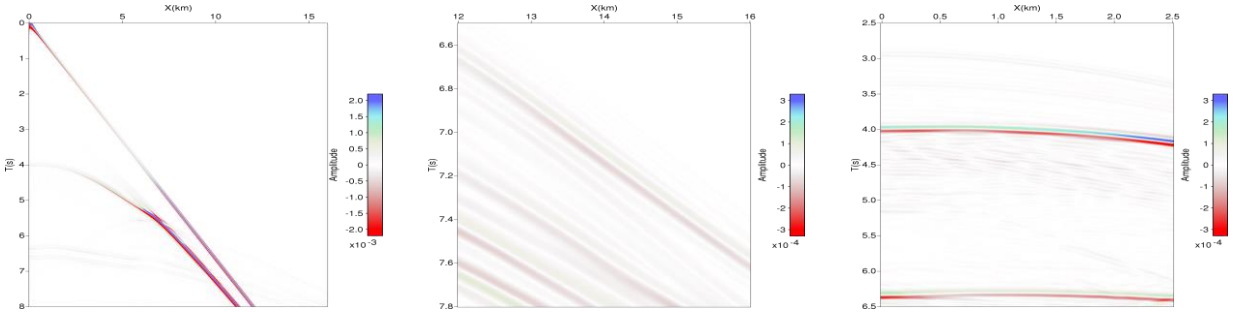

(g) Residue correction 3 (h) Residue correction 3 (far) (i) Residue correction 3 (near)

Figure 7: Comparison between proposed corrections for 3D data to 2D, for a reference shot-gather.

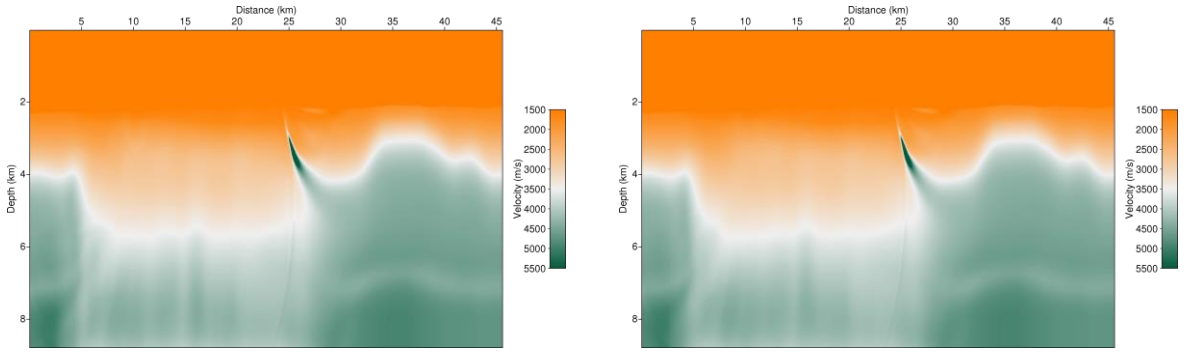

(a) 2.5D data (b) 3D data

Figure 8: 2D FWI result with L_2 norm without amplitude correction.

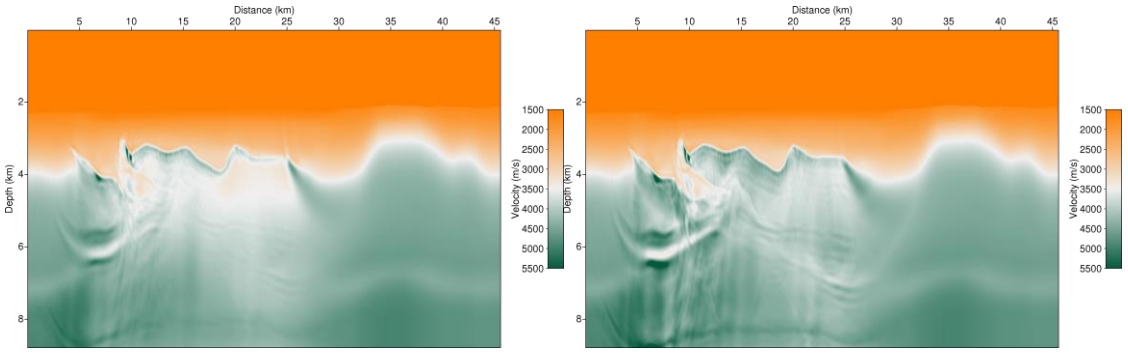

(a) FWI L_2: 2.5D data & Correction 1 (b) FWI L_2: 3D data & Correction 1

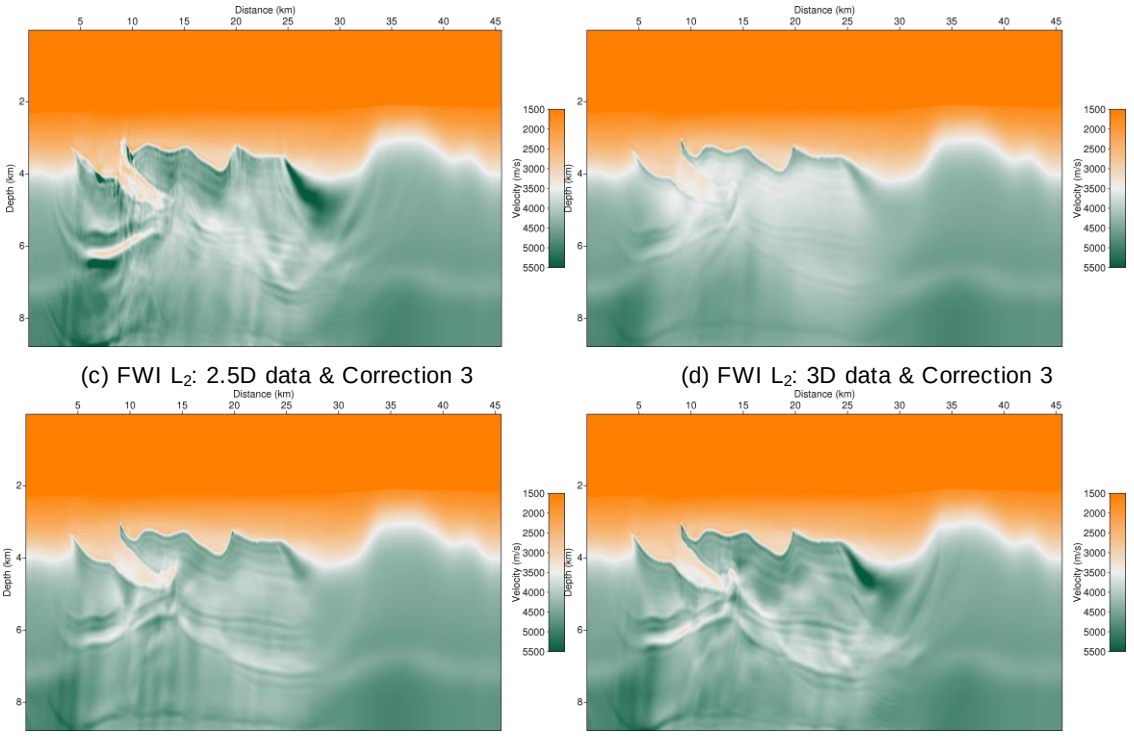

(c) FWI L_2: 2.5D data & Correction 3

(d) FWI L_2: 3D data & Correction 3

(e) FWI $L_{2\text{-rms}}$: 2.5D data & Correction 3

(f) FWI $L_{2\text{-rms}}$: 3D data & Correction 3

Figure 9: Comparison of FWI results with 2.5D and 3D data with different amplitude correction and optimization norm.

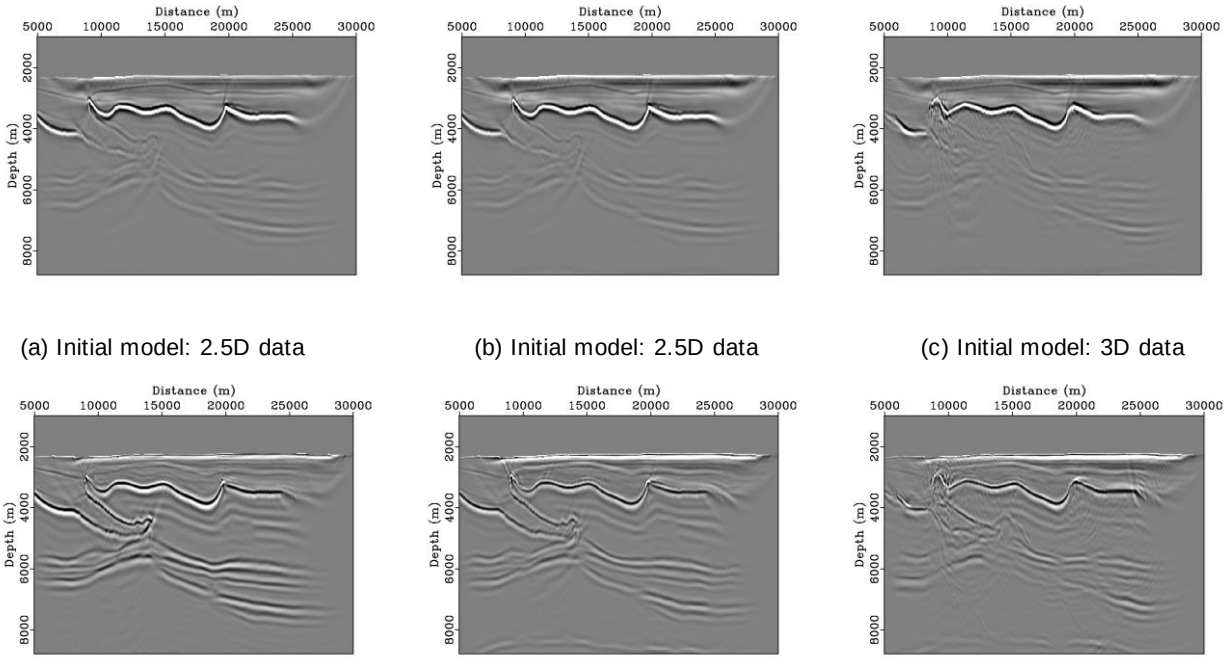

(a) Initial model: 2.5D data

(b) Initial model: 2.5D data

(c) Initial model: 3D data

(d) FWI model: 2.5D data

(e) FWI model: 2.5D data

(f) FWI model: 3D data

Figure 10: Comparison between different RTM images for 2D, 2.5D and 3D models, with the initial and the FWI model (best case -- FWI $L_{2\text{-rms}}$ & correction 3). For all cases, it is clear the benefit gained from the utilization of the FWI model, especially in the pre-salt region.